

Computation of Heat Transfer from an Impinging Flame Jet to a Plane Surface

John J. Kreuder*, Allan T. Kirkpatrick† and Xinfeng Gao‡

A computational fluid dynamics and heat transfer analysis is performed to determine the convection and radiation heat transfer from an impinging flame jet to a plane surface. This paper focuses on analyzing the behavior of an impinging flame jet, including buoyancy effects, turbulence influence, and convective and radiative heat transfer processes. The combustion is modeled using a 12-species probability density function method for the reaction of a single hydrocarbon fuel species $C_{12}H_{23}(l)$. The Reynolds-averaged Navier-Stokes with SST $k - \omega$ turbulence model and large eddy simulation with the Smagorinsky-Lilly sub-grid scale model are used to resolve the turbulent behavior of the impinging flame jet. The discrete ordinates radiation model is employed to determine radiative heat transfer to the impingement surface. Gas emissivity is estimated using the weighted sum of gray gasses model. Liquid fuel droplets interact with the turbulent gas medium in accordance with the discrete random walk model.

Large eddy simulation and Reynolds-averaged Navier-Stokes simulations are carried out using a commercial computational fluid dynamics code. The behavior of the jet is compared with literature data for validation. The results include the convective and radiative components of the total heat flux, as well as local Nusselt numbers and other primary solution variables throughout the flow field.

Nomenclature

Arabic Symbols

$C_{p,n}$	specific heat of species n
h	local convection coefficient
k_m	mixture thermal conductivity
Nu	local Nusselt number

Greek Symbols

ϵ_m	mixture average emissivity
κ	specific turbulence kinetic energy
μ_m	mixture dynamic viscosity
ω	specific dissipation rate

I. Introduction

The objective of this paper is to determine the convection and radiation heat transfer from a turbulent impinging flame jet to a plane surface. Impinging jets have many applications in heat transfer, including materials flammability testing and certification, heat treatment, turbine blade cooling, and electronics cooling. For example, knowledge of the heat transfer from a flame is needed to determine the ignition threshold of combustible materials.

The United States Federal Aviation Administration (FAA) specifies a modified oil burner to simulate the effects of an external fuel fire on an aircraft fuselage and interior components.¹ The specified burner is a typical home heating oil burner fueled by Jet-A fuel at a flow rate of 2.0 gallons per hour. The burner flame characteristics, a minimum average flame temperature and heat flux, are scaled from measurements made

*Ph.D. Candidate, Colorado State University, Department of Mechanical Engineering, Fort Collins, Colorado, 80523, USA, Student AIAA Member.

†Professor, Colorado State University Department of Mechanical Engineering, Fort Collins, Colorado, 80523, USA, AIAA Member.

‡Assistant Professor, Colorado State University, Department of Mechanical Engineering, Fort Collins, Colorado, 80523, USA, AIAA Member.

from full scale pool fire testing. In this paper we develop a CFD model of this oil burner for computation of the impinging flame heat transfer.

The governing parameters of this problem include the flame type (diffusion or premixed), fuel type, equivalence ratio, jet Reynolds number, and nozzle-surface separation distance. The flow field of an impinging jet can be classified into three general regions, a free jet region at the nozzle exit, a stagnation region where the jet flow stagnates and turns parallel to the surface, and a wall jet region where the jet flow is along the wall surface.

I.A. Review of Literature

There have been many investigations of jet impingement. A general review of jet impingement heat transfer is given in Zuckerman and Lior,² and a review of heat transfer to impinging isothermal gas and flame jets is given in Viskanta.³ An overall review of radiation heat transfer in combustion systems, including flame radiation, was written by Viskanta and Menguc.⁴ Semi-empirical correlations for flame impingement heat transfer are reviewed in Baukal and Gebhart.⁵

Angioletti et al.⁶ performed CFD modeling of jet impingement with three different turbulence models and compared the resulting local Nusselt number distributions with experiment. An example of a recent study is Singh et al.,⁷ who measured the effect of Reynolds number, separation distance, and equivalence ratio on the surface heat flux distribution. A hot jet will experience buoyant forces that induce a curvature to the trajectory of the jet. Jirka⁸ has shown that the jet trajectory can be quantified using a relation between the jet's momentum and the buoyant force acting on the jet.

Jet fuels are chemically very complex, with more than 300 components, so their oxidation involves a large number of reaction species. A reduced chemistry (12 species, 13 steps) model for the finite rate combustion of Jet-A has been developed by Kundu et al.⁹ In an early paper, Fu¹⁰ measured the heat radiation from free burning aviation fuels. More recently, Jensen et al.¹¹ compared six different computational methods, including discrete ordinates model (DOM), discrete transfer model, and Monte Carlo, for the solution of the radiative transfer equation in jet fuel fires, and found that the DOM method agreed well with reference solutions.

II. Computational Model

II.A. Chemical Kinetics and Turbulence-Chemistry Interaction Modeling

The thermophysical properties of a combusting gas mixture are dependent on both temperature and local composition. In this paper, specific heats of all species are determined using piece-wise polynomial curve fits in Eqn. 1; the mixture specific heat is then determined by applying a mixing law. Other fluid properties, namely the mixture molecular viscosity (μ_m) and thermal conductivity (k_m), are approximated by a linear function of temperature, shown in Eqn. 2-3.¹²

$$C_{p_n} = A_n + B_n T + C_n T^2 + D_n T^3 + E_n T^4, \quad (1)$$

$$\mu_m = 1.127 \times 10^{-8} T + 3.094 \times 10^{-5}, \quad (2)$$

$$k_m = 5.395 \times 10^{-5} T + 0.013, \quad (3)$$

where the terms A_n , B_n , C_n , D_n , and E_n are empirical constants of the piece-wise function $C_{p_n}(T)$, defined in two temperature ranges: $300\text{K} \leq T \leq 1000\text{K}$ and $1000\text{K} \leq T \leq 5000\text{K}$.

The burner fuel is represented by $\text{C}_{12}\text{H}_{23}$ and a 12-species model is used to describe the combustion reaction. We consider non-premixed combustion, since fuel and oxidizer enter the reaction zone in distinct streams. For modeling of the turbulence-chemistry interaction, the finite rate eddy dissipation concept (EDC) model and the assumed-shape probability density function (PDF)¹³ approach were investigated. In the case of the EDC model, the 13-step mechanism of Kundu⁹ is used to prescribe the finite rate chemistry. For the PDF model, an equilibrium assumption is employed and the finite rate chemistry is not involved. We have investigated both the EDC model and the PDF approaches and found the latter produces adequate predictions at a smaller computational expense. Results reported in Section IV are based on a 12-species equilibrium model using the PDF approach.

II.B. Turbulence Model and Turbulence-Spray Interaction

Radiation, chemical kinetics, and turbulence effects are individually among the most challenging fundamentals for computational combustion modeling, so performing coupled simulations is computationally expensive. An unsteady Reynolds-averaged Navier stokes (RANS) study was carried out first and then a large eddy simulation (LES) investigation followed using information derived from the RANS simulations. In the RANS simulations, the two-equation SST $k-\omega$ model of Menter¹⁴ is used to model the unresolved turbulent flow quantities. For LES, the Smagorinsky-Lilly sub-grid scale model is used.

In consideration of the liquid kerosene fuel, a turbulent spray combustion process is involved. This process is complicated by various physical phenomena including particle dispersion, vaporization, mixing and combustion. The interaction between turbulence and spray is modeled by a stochastic tracking (discrete random walk) model that includes the effect of turbulence intensity on the particle trajectories. The discrete random walk model is known to give nonphysical results in strongly nonhomogeneous, diffusion-dominated flows. Advanced models describing the turbulence-spray interaction are needed for future work.

The spray nozzle used in the FAA flame test experiment is an 80° Monarch PL type nozzle, which forms a hollow cone shaped spray pattern as shown in Fig. 1(a). The injection site is located at the end of the fuel tube, 0.373m downstream from the air inlet. In this CFD study, droplets are injected at half angles of 35°–40°, at a radial distance of 1.58mm from the x -axis. In order to replicate the PL spray pattern, the initial droplet velocity magnitude is set to 7.25 m/s with a swirl component of 60% of the inlet velocity in the tangential direction. The total fuel injection rate is held at 2.0 gallons per hour, and fuel is injected at a temperature of 300K. The diameter of the droplets is approximately 10 μ m and the droplets have the properties of liquid Jet-A fuel. Figure 1(b) shows that the numerical spray pattern closely resembles the physical one. Representative droplet trajectories resulting from this spray pattern are shown in Fig.2.

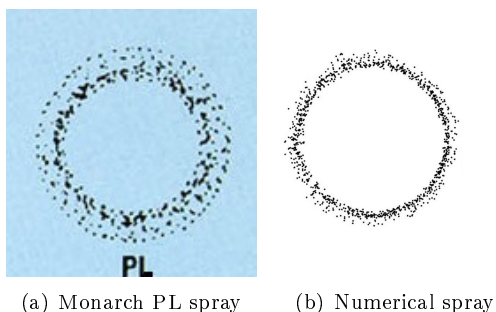


Figure 1. Comparison between the physical and the numerical spray patterns at 10cm downstream from the injection site. Note that the commercial provider does not guarantee consistency in (a) due to the geometric tolerance of the spray nozzles.

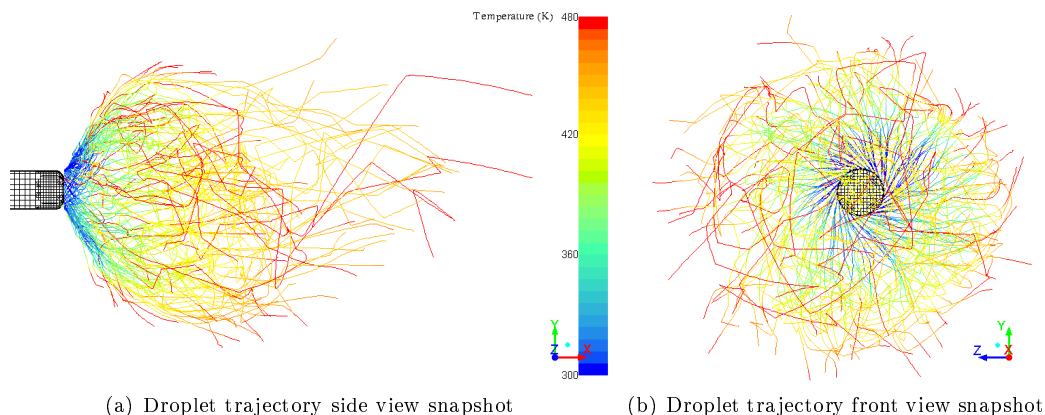


Figure 2. Snapshots of the droplet trajectories colored by temperature. Injector shown in black.

II.C. Radiation Model

Flame radiation can play an important part in the overall combustion and heat transfer process. Previous (4, 15, 16) studies have shown that radiation heat transfer may change the temperature of the flame significantly, which can result in a significant modification of the chemical kinetics and species distribution (NO_x , CO, or soot formation). Moreover, impinging flames are often turbulent; consequently, another important question is to what extent the turbulence and radiation interaction will modify the flow properties, the radiative heat transfer, and the temperature field in the flame. Conversely, the chemical reactions, species concentrations, and flame structure will also be affected. In addition, we need to obtain detailed information on the radiative properties of the combustion mixtures to determine the radiation heat transfer from the flame to a surface.

For the prediction of multidimensional radiative heat transfer in participating media, the discrete ordinates model (DOM) has been one of the most widely applied methods. It requires a single formulation to invoke higher order approximations and is applicable to non-gray¹⁷ and anisotropically scattering media.¹⁸ Based on these characteristics, the DOM is employed for the simulations performed herein.

The radiative properties (absorptivity and emissivity) of a combustng gas mixture depend primarily on local chemical composition, absorption bands of gas constituents, local pressure, local temperature and gas geometry. A comprehensive radiation model that accounts for the absorption bands of each species can be computationally expensive, while a gray gas model approach is likely to be oversimplified. A compromise between the two models is the weighted sum of gray gasses model (WSGGM). In this study, we adopted the WSGGM to calculate radiative heat transfer. The model calculates the local emissivity of the gas mixture using Eqn. 4 to account for the dependence on temperature and composition.

$$\epsilon_m = \sum_{i=0}^I f_{\epsilon,i}(T)(1 - e^{-\epsilon_i(T)ps}) \quad (4)$$

In this formulation, the $f_{\epsilon,i}(T)$, described in Smith and Friedman,¹⁹ is the weighting factor for each of the participating species in the gaseous mixture. The average emissivity $\epsilon_i(T)$ of each participating species is given by Copalle and Vivisch²⁰ as a function of temperature. The local pressure is p , and the mean beam length is denoted by s . The mean beam length is calculated for a generic gas geometry using $s = 3.6V/A$,²¹ where V is gas volume and A is the radiation surface area. Radiation from soot particles is not considered in these simulations.

II.D. Computational Domain, Boundary Conditions, and Mesh

The modified oil burner model under investigation is a Carlin 200¹, typically used in aviation fuel flammability testing. The domain of the computational configuration is shown in Fig. 3, consisting of a draft tube, diffuser cone and quiescent exhaust region. The diameter of the draft tube is 10 cm, and its length is 30 cm. The fuel tube, with a diameter of 3.15 mm, runs along the center of the draft tube and extends into the draft tube a distance of 0.373m, terminating at the fuel nozzle. In experiments, combustion is initiated by a spark ignitor located just downstream from the fuel inlet, producing a flame which stabilizes in the diffuser cone, extending into the quiescent environment downstream and impinging onto a test specimen.

The computational mesh shown in Fig. 4 is created using the cut-cell method provided by the commercial software package Ansys 14.0®. A series of meshes were studied and a grid-independent solution was achieved with a mesh size of 2.8 million cells. Recall that this study is interested in performing simulations for a flame jet in both impinging and non-impinging scenarios. For studying the impinging flame, a flat plate measuring 12 in.×6 in.×0.75 in. is mounted 4 inches downstream of the diffuser outlet as illustrated in Fig 3. The center of the impingement surface is elevated 1 inch above the center line of the diffuser cone to compensate for buoyant effects in the hot jet. For non-impinging simulations, the plate is removed. A 1 inch diameter calorimeter is mounted at the center of the flat marinite plate. Detailed information on the dimensions can be seen in Fig. 5.

Figure 3 shows the computational domain and different types of boundaries are labeled. At the inlet (1), the air mass flow rate is specified as 0.06 kg/s. A swirl component is added to the velocity, $\vec{v} = \bar{u}(0\vec{v}_r + 0.8\vec{v}_\theta + 0.6\vec{v}_z)$, to emulate the physical swirler effect. The inlet temperature is maintained at 300K and turbulence intensity is approximately 10%. An adiabatic, no-slip condition is applied to all the walls (2-5 and 7). The thermal boundary condition for the plate surface (5) is implemented by energy balance, except

the surface of the calorimeter (4), which is treated as an isothermal surface at 300K. The back pressure is specified for the far-field boundaries. In addition, the emissivity for the solid walls (2, 3, and 7) is 0.05, and those for 4 and 5 are 0.95, and 0.7, respectively.

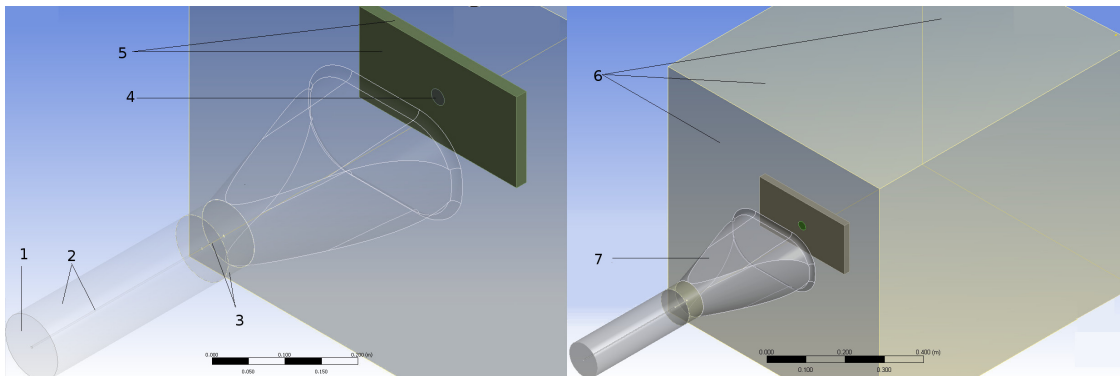


Figure 3. A computational domain represents the physical geometry as described by the FAA.¹

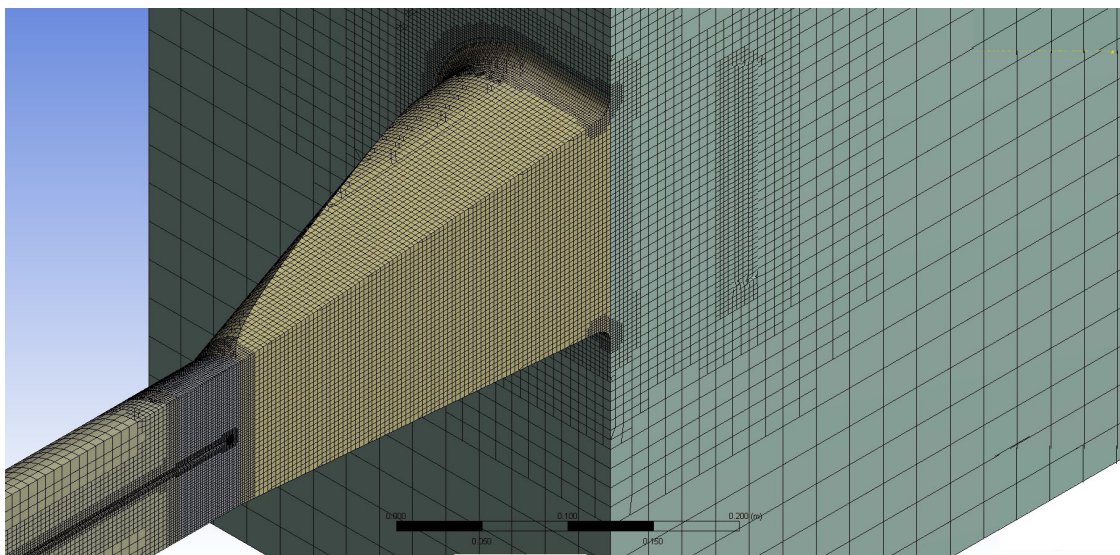


Figure 4. A base mesh of about 0.5 million cells shows the adaptive grids in regions of interest.

III. Validation

Flame test simulations are performed using the commercial software package FLUENT[®] for the three-dimensional turbulent flow fields, both non-reacting and reacting. The numerical scheme is second order in both time and space. An implicit time-marching method is employed and the default under-relaxation factors are decreased by 30% to 50% to facilitate convergence in each time step. In transient simulations, a converged steady solution was used as an initial condition, since our interest is to study the flame jet behavior and associated heat transfer processes at a statistically steady state. The integral time scale of the flow in the combustion region is calculated to be on the order of 10 ms. Using this information, a time step of 1 ms is chosen for the large eddy simulation. For the RANS case, adaptive time stepping is allowed, with each time step size limited to no less than 1 ms.

We first performed simulations of a hot free jet in the absence of any combustion. The free jet prediction is compared to Jirka⁸ as shown in Fig. 6. The centerline trajectory of a buoyant jet in a quiescent medium can be determined as a function of the jet momentum and buoyant force. We observed good agreement between the predicted jet trajectory and data from the literature. Simulation results for the impinging jet were compared with published data from Malmstrom et al.²³ and Angioletti et al.⁶ to establish a baseline for further jet simulations. Good agreement was observed when comparing flow fields and heat transfer.

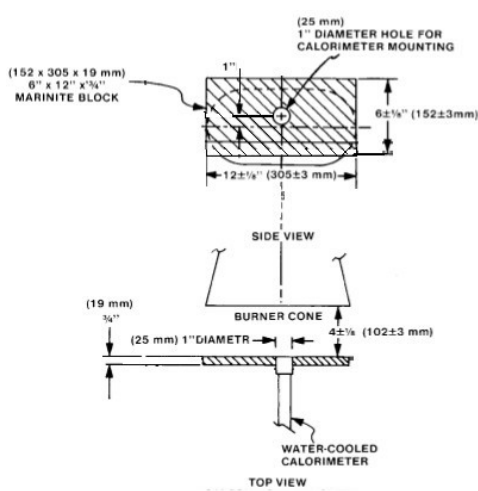


Figure 5. Detailed geometry of calorimeter and impingement surface²²

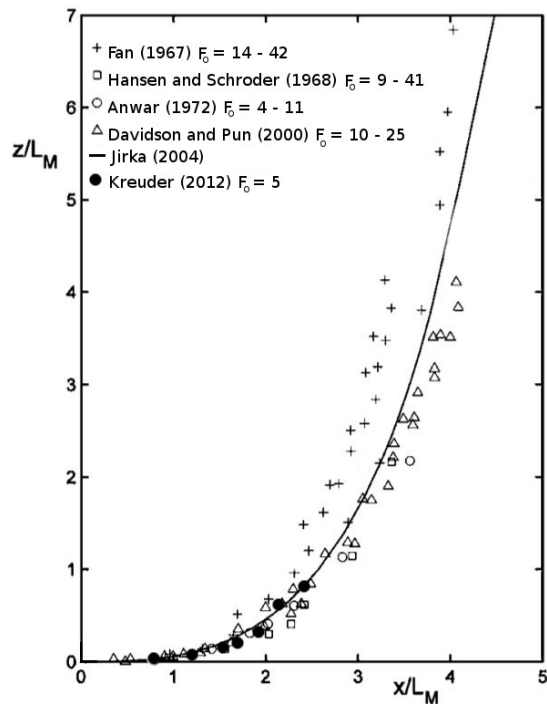
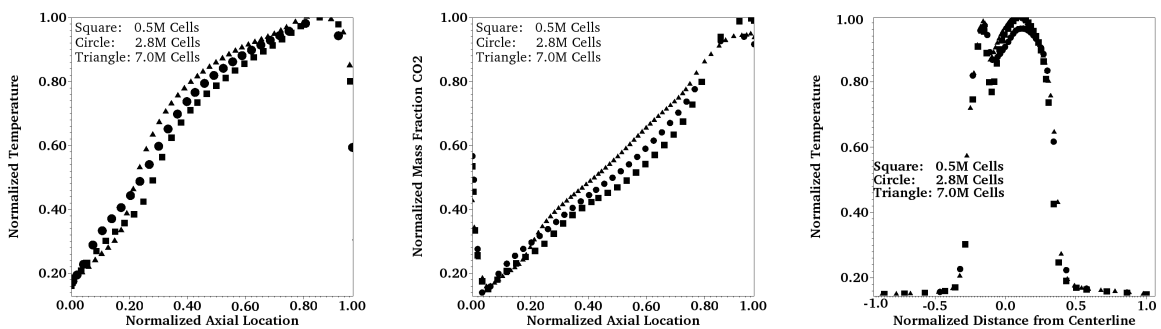


Figure 6. Comparison of the buoyant jet trajectory against data from Jirka⁸

In subsequent simulations, the 12-species PDF combustion model described in Sec. II.A is used. A grid independence study is performed on results from the impinging jet case. Analogous steady state flame simulations are carried out on meshes containing 0.5 million, 2.8 million and 7 million cells, respectively. Figure 7 shows selected results of the grid independence study. From this it is evident that the variation in the primary solution parameters, temperature and CO₂ mass fraction, becomes small as the mesh is refined. For subsequent transient impinging simulations, the 2.8 million cell mesh is used.



(a) Normalized axial temperature in the mid plane (b) Normalized axial mass fraction of CO₂ in the mid plane (c) Normalized temperature along the impingement surface

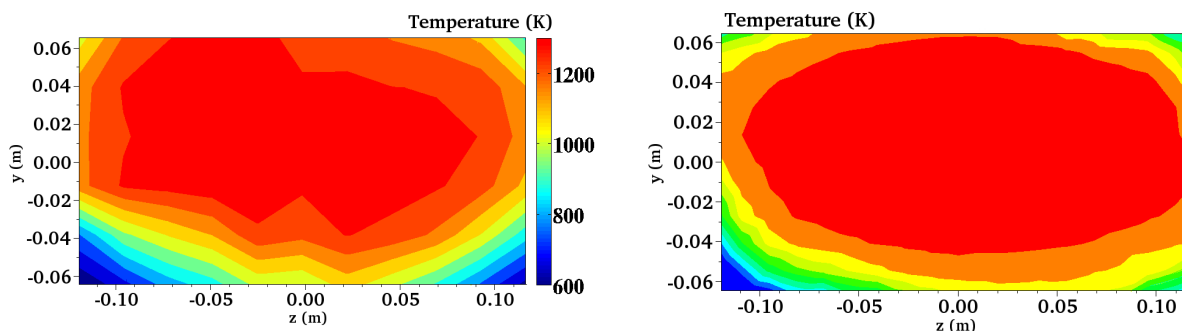
Figure 7. A comparison of the primary solution parameters from three grids.

We also carried out a steady-state bluff-body burner combustion simulation and compared results to the computational study in Gao²⁴ and the experimental data from Masri et al.^{25,26} The purpose is to gain confidence in the solution procedure and choice of numerical parameters when simulating this practical oil burner. The computational configuration and boundary conditions for the bluff-body burner are described in Gao.²⁷ The case considers the non-premixed combustion of methane with a simplified chemical kinetics mechanism. The predicted mean flow quantities (velocity, temperature, and major species concentration) and turbulent fluctuations (turbulent kinetic energy and root mean square of velocity) at the center line of

the bluff-body burner and various radial profiles at a number of locations from the burner base were in good comparison to the literature data both computational and experimental.

IV. Results

We present here the analysis of the simulations for the oil burner flame configuration as described in Section II.D. Two cases, a free flame jet and an impinging flame jet, were investigated. Results are shown for time at approximately 2.0s including the temperature and velocity fields, as well as chemical species concentrations. Note that the transient case was initialized from a converged steady state impinging flame simulation since we are interested in analyzing the solution at a statistical steady state. A 2.0 second simulation represents more than 100 eddy turnovers on the integral scale. The convection and radiation components of the heat flux for the impingement case are also presented. For the impinging flame, simulations were also performed using LES and the results are presented alongside the RANS results. The free flame jet is primarily used to determine an appropriate air flow rate. The FAA allows additional air to be supplied to the reacting system in order to lower the flame temperature into the required range of 1255K to 1366K as measured by 1/16 inch metal sheathed, ceramic packed, type K, grounded thermocouples (with a nominal 22 to 30 American wire gage (AWG)-size conductor). The seven thermocouples must be attached to a steel angle bracket to form a thermocouple rake for placement in the test stand about 10 cm downstream from the outlet of the diffuser cone during burner calibration. The seven thermocouples are equally spaced 1 inch apart, forming a 6 inch thermocouple rake. The thermocouples do not effectively mitigate heat loss by radiation, and therefore underpredict the actual flame temperature.

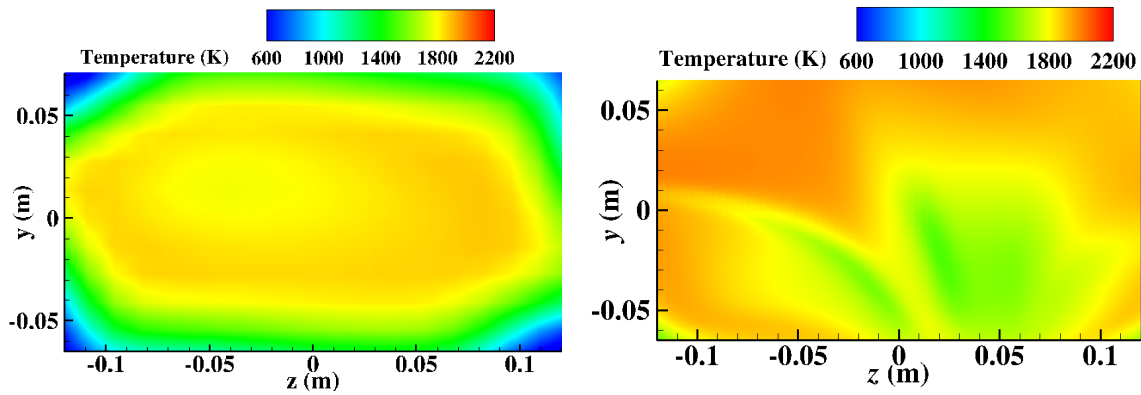


(a) Experimental temperature measurements made by 1/16 inch metal sheathed, ceramic packed, type K, grounded thermocouples. (b) Temperature contour predicted by RANS simulation, assuming zero emissivity of the gas mixture for the free flame jet

Figure 8. Temperature contours in the transverse plane with an axial location at the 10cm downstream from the diffuser cone outlet from experimental data and numerical data of the free flame jet, respectively.

An experimental temperature field provided by the FAA¹ is shown in Fig. 8(a). Through the simulations of the free flame jet, we found that an air flow rate of 0.060 kg/s results in a temperature field that falls within the acceptable range. Figure 8(b) shows the resulting transverse temperature profile from a free jet simulation, assuming zero emissivity in the combusting gas. By adjusting the air flow rate, we reproduced the FAA’s experimental temperature results as shown in Fig. 8. However, the radiation heat exchange between the impingement surface and the surrounding surface exists and has been taken into account in the simulation. When the gasses in the system are treated as participants in the radiation calculation, higher temperatures result. The corresponding transverse temperature profile for the free flame jet is shown in Fig. 9(a) and a maximum temperature of 1800K is observed. When an impingement surface is added at the same location, a steeper temperature gradient field is observed. This temperature distribution may be a result of the impact of the flow structure along the impingement surface as shown in Figs. 11(c)–11(d). For illustrative purposes, a 3-dimensional rendering of the flame produced by the LES simulation is shown in Fig. 10(a). A temperature contour at the plane located at 10cm downstream from the diffuser cone outlet is plotted in Fig. 10(b) to compare with the RANS results at the exact physical location. As expected, the LES simulation produces results on a finer scale; however, Figure 9(b), a RANS averaged temperature profile, does not resemble Fig. 10(b), a snapshot of the LES temperature field. A statistical mean profile needs to be obtained over a time interval from the LES result.

The FAA flame test also requires that a heat flux about 10.5 BTU/(ft²·s) should be measured by a Gardon



(a) Temperature contour predicted by RANS simulation, (b) Temperature contour predicted by RANS simulation, assuming emissivity of the gas mixture based on Eqn.4 for the free flame jet

Figure 9. Temperature contours in the transverse plane with an axial location at the 10cm downstream from the diffuser cone outlet for the free and the impinging flame jet, respectively.

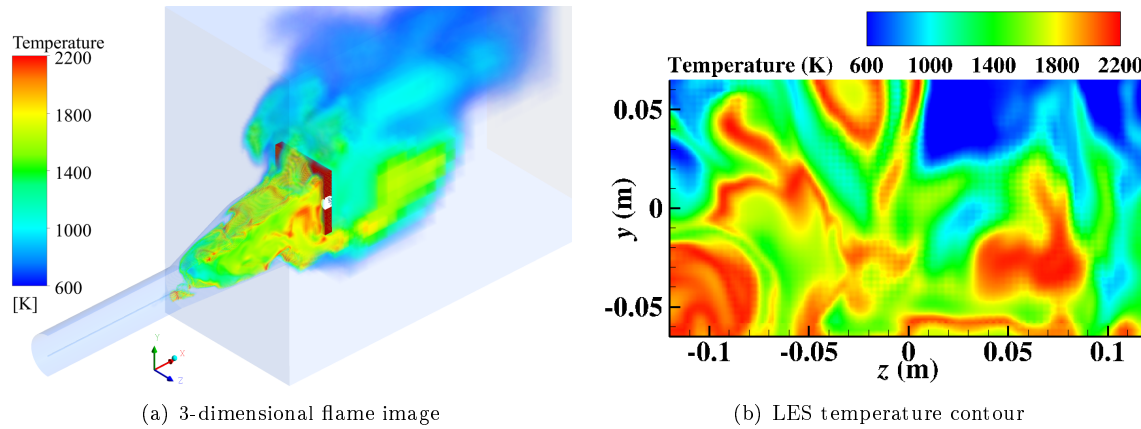


Figure 10. A 3-dimensional flame rendering beginning at the mid-plane, showing flame structure as predicted by LES (a) and Temperature contour predicted by LES, assuming emissivity of the impinging gas mixture based on Eqn.4 at a location 10cm downstream from the diffuser cone outlet (b).

gauge water cooled calorimeter. In our simulations, the calorimeter surface is treated as an isothermal surface at 300K. The resulting flow and temperature fields for the impinging flame jet were computed by both LES and RANS simulations. Selected primary solution variables are plotted in the vertical mid-plane for both simulations and they are displayed in Figs. 11 and 12. Again, it is expected that the LES captures finer flow structures while the RANS provides the mean profile. The experimental setup²² requires that the center of the impingement surface is vertically offset a distance of 1 inch from the centerline in the y -direction to account for the flame buoyancy effect. The numerical simulation does verify this necessity. Additional interesting studies for future consideration include varying the plate size, the plate location along the y -direction, and the turbulence level prescribed at boundaries. Moreover, the distribution of CO_2 mass fraction on the selected plane from the RANS does not closely represent an average of the LES result as shown in Fig. 13. We plan to perform a statistical average of a time sequence of LES results to investigate this discrepancy.

We are interested in knowing how much the heat transfer process is influenced by the finer structures resolved by LES. Figure 14 shows the magnitude of the total heat flux from the flame to the calorimeter surface and the component due to radiation, in addition to the local convection coefficient h and Nusselt number Nu_y , as calculated along the vertical diameter of the calorimeter surface. Integrating over the surface, the average heat flux over the entire calorimeter surface is calculated to be around 12 BTU/(ft²·s) for RANS and 10.5 BTU/(ft²·s) for LES at this instant in time. It appears that the radiation component of the heat transfer is approximately half of the total heat flux for both cases. Both RANS and LES simulations

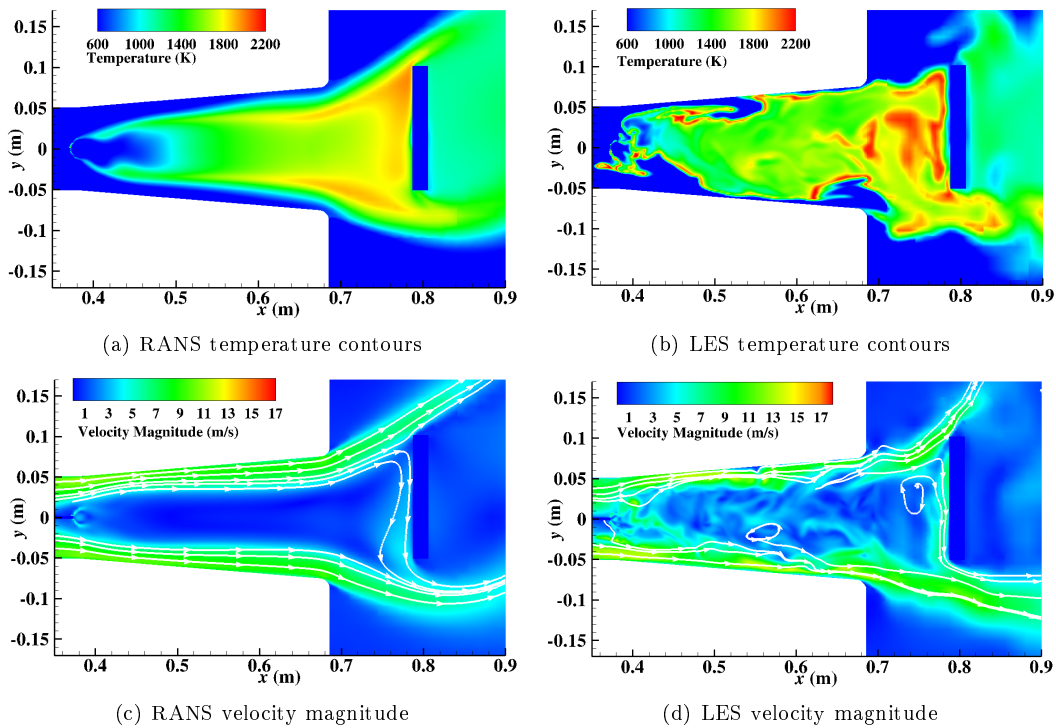


Figure 11. Contours of temperature and velocity on the vertical mid-plane of the domain.

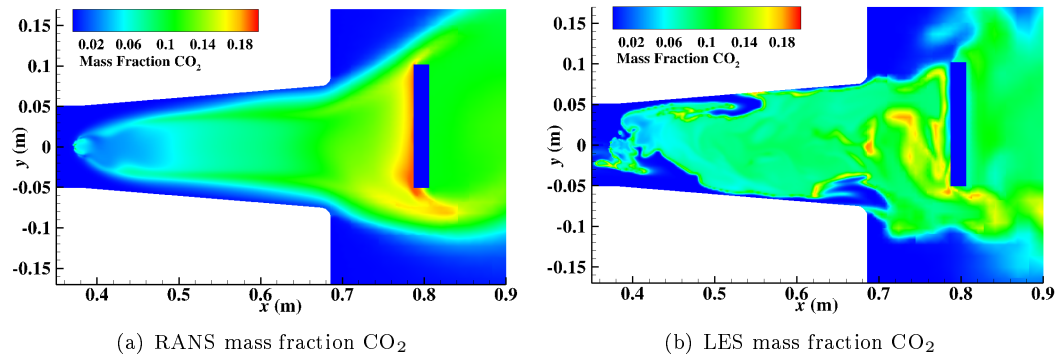


Figure 12. Contour of CO₂ mass fraction on the vertical mid-plane of the domain.

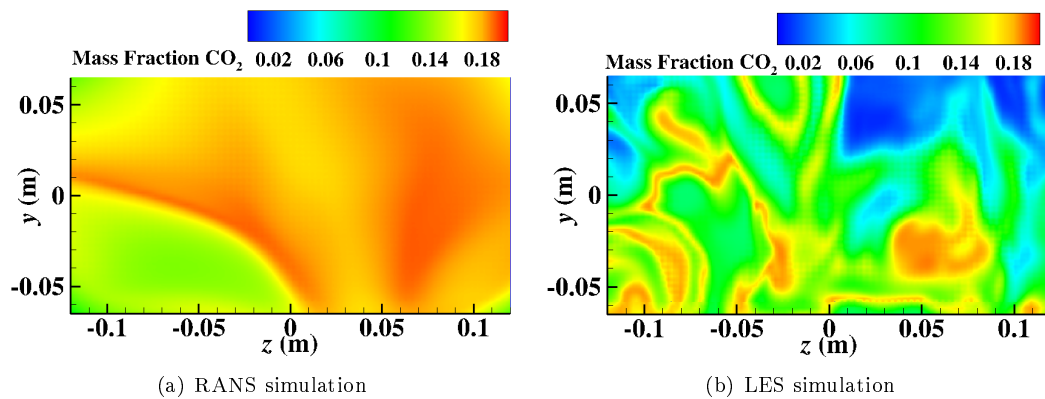


Figure 13. Contours of CO₂ mass fraction on the transverse plane 10cm downstream from the diffuser cone outlet.

predict a fairly uniform heat flux over the calorimeter surface. The RANS case appears to over-predict the heat flux when compared to the LES results, however, a time averaged data set must be generated and analyzed in order to verify this observation. The Nusselt number is calculated as $Nu_y = hy'/k$, where y' is equal to the vertical distance from the stagnation point and k is the local thermal conductivity of the gas. Figure 14(b) shows that exceptional agreement is achieved for the values of h and Nu_y between the two simulations. Immediate follow-up work will be to correlate the flame temperature with the radiative heat transfer from the flame.

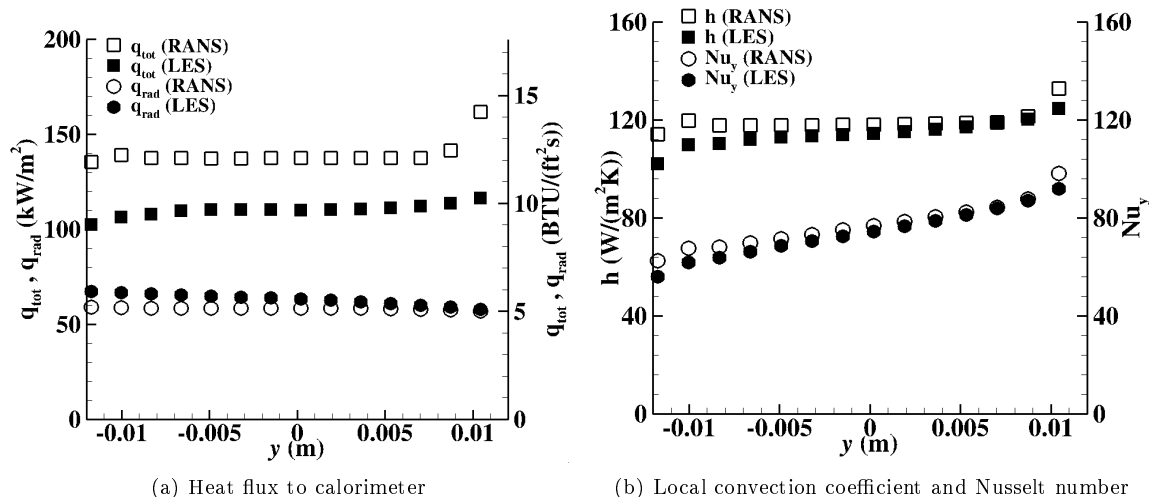


Figure 14. Total heat flux (q_{tot}) and radiation heat flux (q_{rad}) along the vertical diameter of the calorimeter and the local heat transfer coefficient h and Nusselt number Nu_y for both the LES and RANS cases.

V. Concluding Remarks and Future Work

We have performed a CFD study of a flame test burner to compute the heat transfer from a turbulent impinging flame jet to a test surface. The convective and radiative heat transfer components of the heat transfer are calculated using both the Reynolds averaged Navier-Stokes and the large eddy simulation approach. The results allow us to develop a more accurate procedure for heat transfer analysis of FAA test burners. This investigation is a prelude to our overarching goal of implementing advanced radiative models in our in-house numerical algorithms for radiation modeling in aviation combustion systems. Future study includes in-depth investigation of turbulence, radiation, and chemistry interaction.

VI. Acknowledgments

The simulations were performed on the Colorado State University IStEC HPC System supported by NSF Grant CNS-0923386.

References

- ¹Demaree, J. E., "Reevaluation of burner characteristics for fire resistance tests," Technical Report FAA-RD-76-213, U.S. Department of Transportation, Federal Aviation Administration, 1977.
- ²Zuckerman, N. and Lior, N., "Jet impingement heat transfer, physics, correlations and numerical modeling," *Adv. Heat Transfer*, Vol. 39, 2006, pp. 565–631.
- ³Viskanta, R., "Heat transfer to impinging isothermal and flame jets," *Exp. Thermal and Fluid Sci.*, Vol. 6, 1993, pp. 111–134.
- ⁴Viskanta, R. and Menguc, M., "Radiation heat transfer in combustion systems," *Prog. Energy Combustion Sci.*, Vol. 13, 1987, pp. 97–160.
- ⁵Baukal, C. and Gebhart, B., "A review of semi-analytical solutions for flame impingement heat transfer," *Int. J. Thermal Sci.*, Vol. 39, 1996, pp. 2989–3002.
- ⁶Angioletti, M., Nino, E. and Ruocco, G., "CFD turbulent modeling of jet impingement and its validation by PIV and mass transfer measurements," *Int. J. Thermal Sci.*, Vol. 96, 1992, pp. 1388–1392.

- ⁷Singh, G., Chander, S., and Ray, A., "Heat transfer characteristics of natural gas/air swirling flame impinging on a flat surface," *Exp. Thermal Fluid Science*, in press, 2012.
- ⁸Jirka, G., "Integral model for turbulent buoyant jets in unbounded stratified flows. part I: single round jet," *Environmental Fluid Mechanics*, Vol. 4, 2004, pp. 1–56.
- ⁹Kundu, K., Penko, P., and Yang, S., "Simplified Jet-A/Air combustion mechanisms for calculation of NOx emissions," *AIAA paper 98-3986*, 1998.
- ¹⁰Fu, T., "Heat radiation from fires of aviation fuels," *Fire Technology*, 1972, pp. 54–67.
- ¹¹Jensen, K., Ripoll, J., Wray, A., Joseph, D., and El-Hafi, M., "On various modeling approaches to radiative heat transfer in pool fires," *Combustion and Flame*, Vol. 148, 2007, pp. 263–279.
- ¹²Turns, S. R., *An Introduction to Combustion*, McGraw-Hill, New York, 2nd ed., 2000.
- ¹³Pope, S. B., "PDF methods for turbulent reactive flows," *Prog. Energy and Combustion Sci.*, Vol. 11, 1985, pp. 119–192.
- ¹⁴Menter, F. R., "Zonal two equation k - ω turbulence models for aerodynamic flows," *AIAA Paper 93-2906*, 1993.
- ¹⁵dos Santos, R., Lecanu, M., Ducruix, S., Gicquel, O., Iacona, E., and Veynante, D., "Coupled large eddy simulations of turbulent combustion and radiative heat transfer," *Combust. Flame*, Vol. 152, No. 3, 2008, pp. 387–400.
- ¹⁶Coelho, P. J., "Approximate solutions of the filtered radiative transfer equation in large eddy simulations of turbulent reactive flows," *Combust. Flame*, Vol. 156, 2009, pp. 1099–1110.
- ¹⁷Fiveland, W. A. and Jamaluddin, A. S., "Three-dimensional spectral radiative heat transfer by the discrete-ordinates method," *J. Thermophys. Heat Transfer*, Vol. 5, No. 3, 1991, pp. 335–339.
- ¹⁸Fiveland, W. A., "Three-dimensional radiative heat transfer solutions by the discrete-ordinates method," *J. Thermophys. Heat Transfer*, Vol. 2, No. 4, 1988, pp. 309.
- ¹⁹Smith, T. Shen, Z. and Friedman, J., "Evaluation of coefficients for weighted sum of gray gasses model," *J. Heat Transfer*, Vol. 104, 1982, pp. 602–608.
- ²⁰Copalle, A. and Vervisch, P., "The total emissivities of high temperature flames," *Combustion and Flame*, Vol. 49, 1983, pp. 101–108.
- ²¹Incropera, F. and Dewitt, D., *Fundamentals of Heat and Mass Transfer*, Wiley, sixth ed., 2007.
- ²²USFAA, "14 CFR Part 25, Airworthiness standatds: Transport category airplanes," Technical Report Appendix F, Part I, 2012.
- ²³Malmstrom, T. G., Kirkpatrick, A. T., Christensen, B., and Knappmiller, K. D., "Centerline velocity decay measurements in low-velocity axisymmetric jets," *J. Fluid Mech.*, Vol. 246, 1997, pp. 363–377.
- ²⁴Gao, X., *A parallel solution-adaptive method for turbulent non-premixed combusting flows*, Ph.D. thesis, University of Toronto, 2008.
- ²⁵Masri, A. R., Dibble, R. W., and Barlow, R. S., "Raman-Rayleigh measurements in bluff-body stabilized flames of hydrocarbon fuels," *Proc. Combust. Inst.*, Vol. 24, 1992, pp. 317–324, Formerly *Twenty-Fourth Symposium (International) on Combustion*.
- ²⁶Masri, A. R., Dally, B. B., and Barlow, R. S., "The structure of the recirculation zone of a bluff-body combustor, in: 25th Symposium on Combustio," *Proc. Combust. Inst.*, Vol. 25, 1994, pp. 1301–1308, Formerly *Twenty-Fifth Symposium (International) on Combustion*.
- ²⁷Gao, X. and Groth, C. P. T., "A parallel solution-adaptive method for three-dimensional turbulent non-premixed combusting flows," *J. Computational Phys.*, Vol. 229, 2010, pp. 3250–3275.